

# Automatic Motion and Noise Artifact Detection in Holter ECG Data Using Empirical Mode Decomposition and Statistical Approaches

Jinseok Lee\*, *Member, IEEE*, David D. McManus, Sneha Merchant, and Ki H. Chon, *Senior Member, IEEE*

**Abstract**—We present a real-time method for the detection of motion and noise (MN) artifacts, which frequently interferes with accurate rhythm assessment when ECG signals are collected from Holter monitors. Our MN artifact detection approach involves two stages. The first stage involves the use of the first-order intrinsic mode function (F-IMF) from the empirical mode decomposition to isolate the artifacts' dynamics as they are largely concentrated in the higher frequencies. The second stage of our approach uses three statistical measures on the F-IMF time series to look for characteristics of randomness and variability, which are hallmark signatures of MN artifacts: the Shannon entropy, mean, and variance. We then use the receiver-operator characteristics curve on Holter data from 15 healthy subjects to derive threshold values associated with these statistical measures to separate between the clean and MN artifacts' data segments. With threshold values derived from 15 training data sets, we tested our algorithms on 30 additional healthy subjects. Our results show that our algorithms are able to detect the presence of MN artifacts with sensitivity and specificity of 96.63% and 94.73%, respectively. In addition, when we applied our previously developed algorithm for atrial fibrillation (AF) detection on those segments that have been labeled to be free from MN artifacts, the specificity increased from 73.66% to 85.04% without loss of sensitivity (74.48%–74.62%) on six subjects diagnosed with AF. Finally, the computation time was less than 0.2 s using a MATLAB code, indicating that real-time application of the algorithms is possible for Holter monitoring.

**Index Terms**—Atrial fibrillation (AF), empirical mode decomposition (EMD), Holter recording, motion and noise (MN) artifact detection, statistical method.

## I. INTRODUCTION

WE have recently developed an algorithm for accurate and real-time detection of atrial fibrillation (AF) that is well-suited for continuous ECG monitoring applications [1].

Manuscript received January 21, 2011; revised June 27, 2011 and October 25, 2011; accepted November 5, 2011. Date of publication November 10, 2011; date of current version May 18, 2012. This work was funded in part by the Office of Naval Research work unit under Grant N00014-08-1-0244. *Asterisk indicates corresponding author.*

\*J. Lee is with the Department of Biomedical Engineering, Worcester Polytechnic Institute, MA 01609 USA (e-mail: jinseok@wpi.edu).

D. D. McManus is with the Cardiology Division, Departments of Medicine and Quantitative Health Sciences, University of Massachusetts Medical Center, Worcester, MA 01605 USA (e-mail: mcmanusd@ummc.org).

S. Merchant is with the Scottcare Corporation, Cleveland, OH 44135 USA (e-mail: smerchant@scottcare.com).

K. H. Chon is with the Department of Biomedical Engineering, Worcester Polytechnic Institute, MA 01609 USA (e-mail: kichon@wpi.edu).

Color versions of one or more of the figures in this paper are available online at <http://ieeexplore.ieee.org>.

Digital Object Identifier 10.1109/TBME.2011.2175729

Use of ECG monitors (e.g., Holter monitors) is common in the diagnosis and management of patients with, or at risk for, AF, given the paroxysmal, short-lived, and frequently asymptomatic nature of this serious arrhythmia. Monitoring for AF is important because, despite often being paroxysmal and associated with minimal or no symptoms, AF is associated with severe adverse health consequences, including stroke, heart failure, and death [2]. Our test of accuracy of the AF algorithm was performed on noise-removed test databases, which also consisted of Holter recordings. Certainly, motion and noise (MN) artifacts are significant during Holter recordings and can lead to false detections of AF. Clinicians have cited MN artifacts in ambulatory monitoring devices as the most common cause of false alarms, loss of signal, and inaccurate readings [3], [4].

Previous computational efforts have largely relied on MN artifact removal, and some of the popular methods include linear filtering [5], adaptive filtering [6], [7], wavelet denoising [8]–[10], and Bayesian filtering methods [11]. One main disadvantage of the adaptive filtering methods is that they require a reference signal, which is presumed to be correlated in some way with the MN artifacts. For mitigating this limitation, use of accelerometers to obtain a reference signal has resulted in some success [12], [13]; however, this approach has not been applied to Holter monitors. The wavelet denoising approach attempts to separate clean and noisy wavelet coefficients, but it can be difficult to use since it requires identification of the location of each ECG morphology including the P and T waves [8]–[10]. Bayesian filtering requires estimation of optimal parameters using any variant of Kalman filtering methods: extended Kalman filter, extended Kalman smoother, or unscented Kalman filter [11]. The main disadvantage of the Bayesian filtering approach is the improper assumption that noise has an additive Gaussian probability density function. Further, the method requires R-peak locations for each cycle of ECG data.

While the aforementioned signal processing approaches have been applied, they are not appropriate, and consequently MN artifacts remain a key obstacle to the accurate detection of AF and atrial flutter, which is an equally problematic arrhythmia. A novel method to separate clean ECG portions from segments with MN artifacts in real time is urgently needed for more accurate diagnosis and treatment of clinically important atrial arrhythmias. For our paper, the aim is to detect the presence of MN artifacts; for Holter applications, there are a sufficient number of clean segments in each recording that MN-contaminated segments can be discarded, thereby increasing the specificity of AF identification. Moreover, our AF detection algorithm is

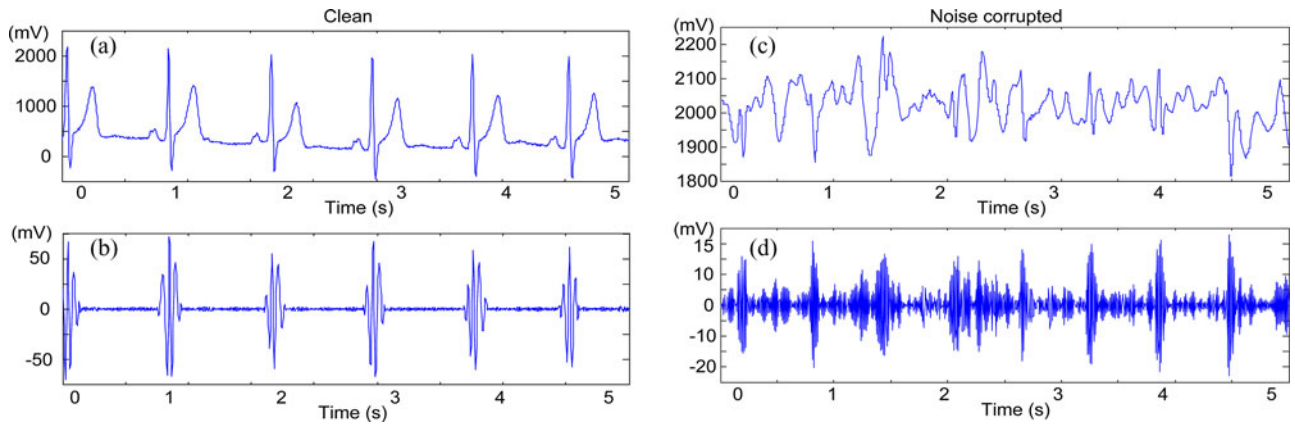


Fig. 1. F-IMF based on clean and noisy ECG signal. (a) Clean ECG signal. (b) F-IMF of the clean signal. (c) Noisy ECG signal. (d) F-IMF of the noisy signal.

based on irregular RR interval dynamics that require accurate identification of R-wave peaks. However, previously developed algorithms involving filtering or signal reconstruction methods are all inappropriate for our application as we need to be certain that the precise timing of the RR interval duration is attained. Reconstruction of ECG waveform algorithms involves estimation procedures, and filtering algorithms may distort the location of R-wave peaks; thus, these algorithms distort RR interval duration calculations and consequently lead to incorrect classification of the presence or absence of AF.

Our MN detection algorithm involves two stages. The first stage of the algorithm involves the use of empirical mode decomposition (EMD) [14] to isolate HF components of the signal under the assumption that they contain most of the MN artifacts' dynamics. The second stage involves calculation of statistical approaches on the high-pass-filtered signal from the first stage to look for signatures of randomness associated with MN artifacts, and the methods utilized include Shannon entropy, mean, and variance values. Specifically, we use the first mode of intrinsic mode function (F-IMF) of the EMD, as the F-IMF of the clean ECG segments have periodic patterns, whereas the MN-artifact-corrupted ECG segments have highly varying irregular dynamics with lower magnitudes. We then obtain an F-IMF threshold value for the separation between clean and MN-corrupted data, derived from 15 healthy subjects with 24-h Holter recordings. With the derived threshold values, we tested the efficacy of the algorithms on 30 different healthy subjects. In addition, we applied the algorithm for AF detection on Holter data from six subjects diagnosed with AF and seven subjects without AF, which were all provided by the Scottcare Corporation, Cleveland, OH.

## II. METHOD

### A. MN Artifact Detection

1) *Algorithm Description*: Our approach to separate clean and noise-corrupted ECG segments starts with EMD. EMD is defined by a process called sifting, and it decomposes any data into a set of IMF components, which become the basis functions for representing the data [14]. It is well known that the IMF basis functions provide a physically meaningful representation

of the underlying processes in many applications [15]–[19]. For our MN artifact detection, we only use a subset of the EMD algorithm, i.e., only the portion of the EMD algorithm that determines the first IMF (F-IMF) is used. Specifically, given a signal  $x(t)$ , the F-IMF is found via the EMD by the following procedure.

- 1) Identify all extrema of  $x(t)$ .
- 2) Interpolate between minima (respectively, maxima) by using a cubic spline and ending up with some envelope  $e_{\min}(t)$  (respectively,  $e_{\max}(t)$ ).
- 3) Compute the mean  $m(t) = (e_{\min}(t) + e_{\max}(t))/2$ .
- 4) Subtract from the signal:  $d(t) = x(t) - m(t)$ .
- 5) Replace  $x(t)$  with  $d(t)$  and iterate the aforementioned steps until  $d(t)$  becomes a zero-mean process. After stopping the iteration,  $d(t)$  is the F-IMF.

It was shown that the dynamics of the F-IMF of the EMD are as though they have been passed through a high-pass filter (HPF) [20]. Hence, it is not surprising that the F-IMF contains dynamics associated with noise for any well-sampled data [21].

The previous statement remains valid for the ECG signal corrupted by MN artifact, i.e., we observe a high-pass filtered signal [see Fig. 1(d)] that has the characteristics of noise dynamics. To illustrate the presence of noise in ECG signal using the F-IMF, we show 5 s of clean and noisy ECG segments from a Holter recording, and the F-IMFs are shown in Fig. 1. The ECG segments were recorded by ScottCare's RZ153 series recorders sampled at 180 Hz with a 10-bit resolution. One segment shown in Fig. 1(a) is noise free without any subject movement, while the other segment shown in Fig. 1(c) is measured with MN artifacts. Fig. 1(b) represents the F-IMF of the clean signal and Fig. 1(d) represents the F-IMF of the noisy signal. It can be seen that the F-IMF of the clean ECG segment has periodic patterns, whereas the MN-artifact-corrupted ECG segment has highly varying irregular dynamics of a lower magnitude than the noise-free ECG signal.

After obtaining F-IMF, we square it since it has both negative and positive values, and then normalize it to a unit value. Note that as the ECG signal amplitudes are different among subjects, who also may have different lead configurations and sensor amplifications, we normalized the squared F-IMF to a unit value. Fig. 2 shows representative squared F-IMF of the clean [see

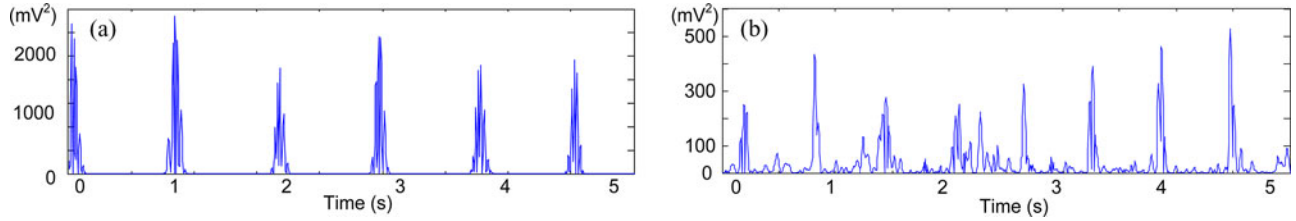


Fig. 2. Squared-IMF based on clean and noisy ECG signal. (a) Clean ECG segment. (b) Noisy ECG segment.

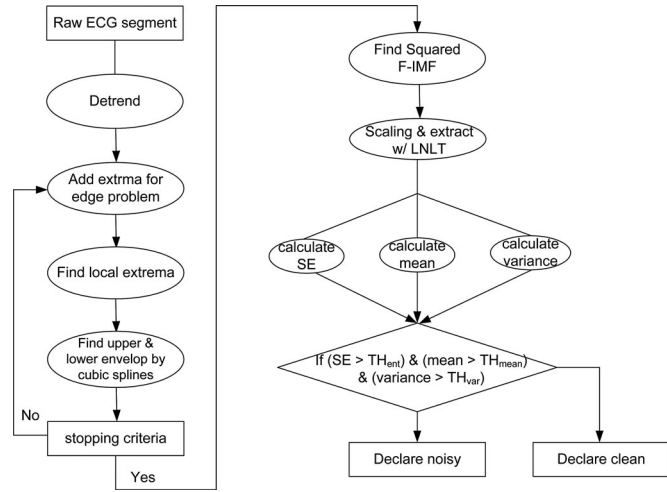


Fig. 3. Simplified algorithm for MN artifact detection in an ECG segment by using EMD and three statistical techniques.

Fig. 1(a)] and noisy signals [see (Fig. 1(b)). As shown in Fig. 2, the peak amplitudes of the clean signal [see Fig. 2(a)] are an order of magnitude higher than those of the MN-corrupted signal [see Fig. 2(b)], indicating that a threshold value can be derived to separate between the two types of signals.

With a normalized squared IMF, we determine the optimum low noise level threshold (LNLT) value and define it as  $TH_{LNLT}$ . For each  $TH_{LNLT}$  value starting from 0 to 1 at an increment of 0.05, we investigate the following three statistical indices: Shannon entropy to characterize randomness, a mean value to quantify LNLT level, and variance to quantify variability. If all values of Shannon entropy, mean, and variance are higher than threshold values of  $TH_{ent}$ ,  $TH_{mean}$ , and  $TH_{var}$ , we declare the segment to be a noise-corrupted segment. The overall algorithm is summarized in Fig. 3. Once  $TH_{LNLT}$  and the thresholds for maximum sensitivity and specificity are determined for each of the three statistical values ( $TH_{ent}$ ,  $TH_{mean}$ , and  $TH_{var}$ ) using the receiver-operator characteristic curve analysis on the data, as described in Section II-B, no further heuristic tuning for the threshold values is required. We also investigated the optimum segment length ( $L_{seg}$ ) for maximum sensitivity and specificity along with computational complexity.

### B. Data Acquisition I: Data Collection and Determination of Optimal Threshold Values

We collected 5-lead ECG Holter recordings (Scottcare Corporation) from 15 healthy subjects. Data were acquired at 180 Hz

with 10-bit resolution for 24 h. None of the subjects had clinically apparent cardiovascular disease. The 15 healthy subjects comprised 8 females and 7 males of age  $31.7 \pm 3.4$  years. During Holter recording, each subject was asked to perform routine daily activities. Among the acquired data, we collected 144 10-s noisy segments, where R-peaks were not clearly recognizable due to MN artifacts. Along with the noisy segments, we collected 144 10-s clean segments, where RR intervals were clearly discernible. Note that the decision to deem a segment noise corrupted or clean was based on the criterion of whether or not the R-peaks of the ECG waveforms were recognizable to the eye.

For the selection of the optimal threshold set consisting of  $TH_{LNLT}$ ,  $TH_{ent}$ ,  $TH_{mean}$ , and  $TH_{var}$ , we searched every possible combination among the 4-D vectors with the following interval increments:

- 1)  $TH_{LNLT}$  varied from 0 to 1 at intervals of 0.05;
- 2)  $TH_{ent}$  varied from 0 to 1 at intervals of 0.0001;
- 3)  $TH_{mean}$  varied from 0 to 1 at intervals of 0.0001;
- 4)  $TH_{var}$  varied from 0 to 0.01 at intervals of 0.00001.

The optimal threshold was determined according to a combination of the four threshold values that provided the best accuracy. The accuracy was calculated as follows:

$$\text{Accuracy} = \frac{TP + TN}{TP + TN + FP + FN} \quad (1)$$

where TP, TN, FP and FN are true positives, true negatives, false positives, and false negatives, respectively. With the data length,  $L_{seg} = 5$  s, we found the accuracy of 0.9688, and the sensitivity and specificity values of 0.9549 and 0.9792, respectively.

1) *Optimal Data Length and Computational Time*: To determine the optimum data length  $L_{seg}$  for MN artifacts detection, we repeated the aforementioned procedure with a segment size varying from 1 to 10 s at an increment of 1 s. Based on each  $L_{seg}$  (1–10 s), we obtained the optimal parameters (e.g., 10 sets of threshold sets) and plotted the accuracy according to  $L_{seg}$ , as shown in Fig. 4(a). The accuracy increased when  $L_{seg}$  increased, but the rate of increase declined when  $L_{seg}$  was equal to or greater than 5 s. In addition, as shown in Fig. 4(b), the computation time for a clean segment linearly increased with the length of data segments. However, the computation time for noisy segments dramatically increased especially when the segment length exceeded 6 s, as shown in Fig. 4(c). Taking into account the computational complexity, we chose the optimum  $L_{seg} = 5$  s. Note that the computational time was obtained by MATLAB 2010a on 2.66 GHz Intel Core2 processor. Table I summarizes the final optimal threshold parameters and

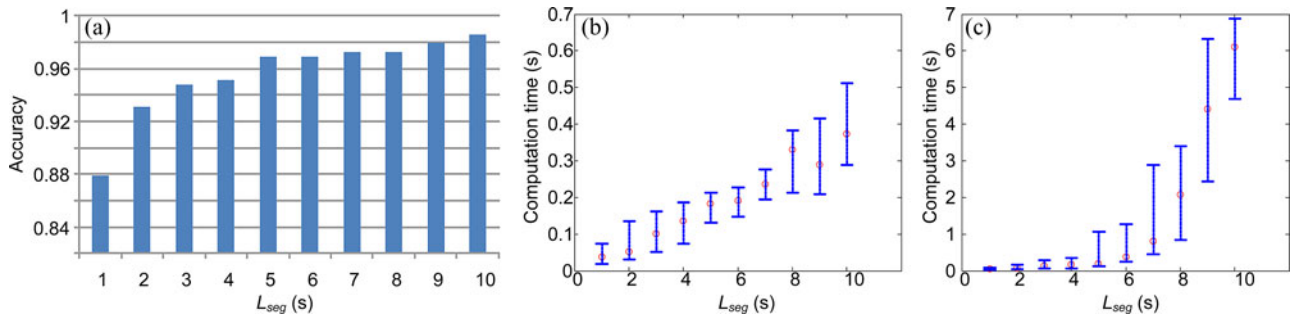


Fig. 4. Effects of segment length: (a) accuracy, (b) computation time with clean segment, and (c) computation time with noisy segment. Whiskers (blue) above and below represent the 90th and the 10th percentiles, respectively, and circle (red) represents median values.

TABLE I  
OPTIMUM PARAMETERS WITH  $L_{seg} = 5$

	$TH_{LNL T}$	$TH_{ent}$	$TH_{mean}$	$TH_{var}$	sensitivity	specificity	accuracy
$L_{seg}=5$ (s)	0.20	0.5998	0.0236	0.00082	0.9549	0.9792	0.9688

the corresponding sensitivity, specificity, and accuracy, where sensitivity and specificity were calculated as follows:

$$\text{Sensitivity} = \frac{TP}{TP + FN} \quad (2)$$

$$\text{Specificity} = \frac{TN}{TN + FP} \quad (3)$$

2) *Comparison of Our Approach to an HPF*: In order to evaluate our algorithm, we compared its performance against a standard HPF. For the HPF, the whole procedure is the same as detailed previously, but we used a squared high-pass-filtered signal instead of the squared F-IMF. We investigated the HPF signal with different cutoff frequencies ranging from 1 to 89 Hz since the data were acquired at 180 Hz. We examined these various  $f_{cut}$  values since the best cutoff frequency to eliminate noise is not known *a priori*. Fig. 5 shows a comparison of the accuracy values [as defined in (3)] for HPF and EMD. We have normalized the highest frequency of 89–0.4944 Hz. As shown in Fig. 5, the accuracy values change as a function of cutoff frequency for the HPF approach. Note that the accuracy can be as low as  $\sim 0.45$  and as high as 0.94, depending on the choice of the cutoff frequency for the HPF, whereas the accuracy for the EMD has a constant value of 0.97 for all frequencies.

### C. Data Acquisition II: Algorithm Verification

In order to verify our algorithm and the threshold values derived from the data, as described in Section II-B, we collected ECG Holter recordings from 30 apparently healthy subjects. All data recordings were collected using ScottCare RZ153 series recorders, and acquired at the sampling rate of 180 Hz with 10-bit resolution for 3 min. The verification sample comprised 15 men and 15 women, with a mean age of  $24 \pm 3.1$  years. None of the verification study sample had clinically apparent cardiovascular disease. During the Holter recording, each subject was asked to stand without any movement for the first 1 min. For the next 1 min, each one was asked to jog. For the last 1 min, each

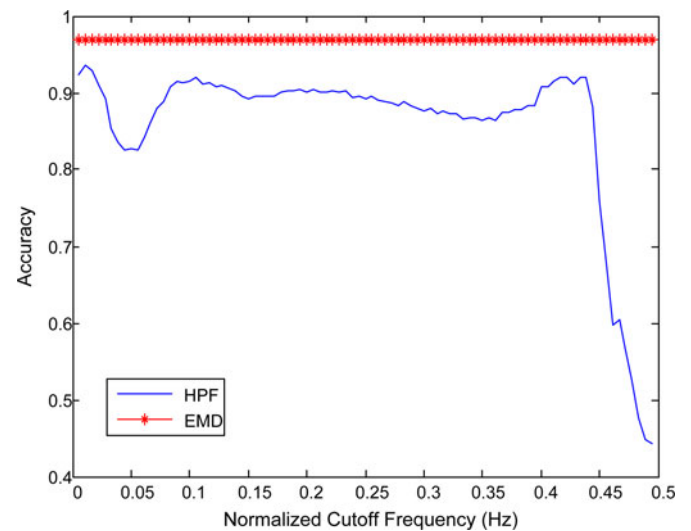


Fig. 5. Accuracy comparison between EMD and HPF with different cutoff frequencies.

one was asked to tap the electrodes attached to their body. Thus, the last 2 min ECG segments were corrupted by MN artifact, while the first 1 min segment was free of noise on the Holter recording. Each data set was categorized into “clean,” “jogging,” and “tapping,” and then tested for MN artifact detection using a MATLAB implementation of our algorithm.

### D. Data Acquisition III: AF Detection

In order to investigate the efficacy of our algorithm using the threshold values derived from the data, as described in Section II-B, we applied the MN artifact algorithms on Holter data from 13 subjects. Six of the thirteen participants had AF, whereas seven participants were in normal sinus rhythm during ECG assessment. These data are from a database provided by Scottcare Corporation. All data were collected using ScottCare RZ153 series recorders with a sampling rate of 180 Hz with 10-bit resolution. Duration of monitoring was 10 min and 24 h for participants in normal sinus rhythm and AF, respectively. The goal of using our MN artifact detection algorithm is to determine how much more accurately the AF detection can be achieved if we do not use those segments that have been identified to contain MN artifacts. In addition, we are also interested in examining

TABLE II  
TP, TN, FP, AND FN BEFORE AND AFTER MN ARTIFACT ELIMINATION BASED ON SEVEN NON-AF SUBJECT DATA SETS

Data	w/ original segment				after MN artifact elimination				Elimination rate (MN artifact detection rate)
	TP	TN	FP	FN	TP	TN	FP	FN	
I	0	573	172	0	0	247	0	0	69.30 %
II	0	686	70	0	0	364	0	0	53.10 %
III	0	666	105	0	0	568	0	0	26.10 %
IV	0	676	10	0	0	611	0	0	9.90 %
V	0	920	5	0	0	864	0	0	6.30 %
VI	0	894	76	0	0	875	0	0	8.48 %
VII	0	518	302	0	0	476	0	0	34.23 %
Overall	0	4933	740	0	0	4005	0	0	
	specificity: 86.96% sensitivity: NA				specificity: 100% sensitivity: NA				

if the MN artifact detection algorithm inadvertently eliminates those segments that have been labeled correctly to contain AF.

The procedure first starts by examining if a data segment contains MN artifacts or not. If the tested segment is corrupted with MN artifacts, then we move on until a segment is found to be free of MN artifacts and subsequently perform our AF detection algorithm, which has been shown to provide accurate AF detection [1].

### III. RESULTS

#### A. Algorithm Verification With Additional Data

Based on additional ECG data from the 30 healthy subjects described in Section II-C, we classified a segment's detection result into one of four possible categories, as given below.

- 1) True negative (TN) = segment detected as "clean" and true annotation is "static."
- 2) True "jogging" positive (TP) = segment detected as "noisy" and true annotation is "jogging" or "tapping."
- 3) False negative (FN) = segment detected as "noisy" and true annotation is "static."
- 4) False "jogging" positive (FP) = segment detected as "clean" and true annotation is "jogging" or "tapping."

We found the sensitivity, specificity, and accuracy to be 0.9663, 0.9473, and 0.9536, respectively. For HPF, the best values of sensitivity, specificity, and accuracy were found to be 0.9447, 0.9451 and 0.9450, respectively, when  $f_{\text{cut}} = 12$  Hz (normalized frequency of 0.07 Hz).

#### B. Non-AF Subject Data Result

Table II shows TPs, TNs, FPs, and FNs of AF detection before and after MN artifact elimination on seven non-AF subjects, as described in Section II-D. Note that data do not include any AF beats; thus, TPs and FNs are zero, and hence, the sensitivity value is not applicable. For *subject I*, an incorrect AF detection was reported 172 times out of 745 RR intervals, but with our MN artifact algorithm, it was determined that 69.30% of the segments were declared to be contaminated by MN artifacts.

Thus, when these MN artifact segments were not analyzed by our AF algorithm, there was no FP detection of AF. Similarly, for *subjects II–VII*, all FP AF detection rates were reduced to zero because they were due to MN artifacts and not AF. Again, the concept is that if MN artifacts are detected in a data segment, then AF detection is not performed, thereby reducing FPs. In summary, inclusion of our MN artifact algorithm increased the specificity from 87% to 100%. For comparison, we applied HPF and found the best specificity of 95.92% when  $f_{\text{cut}} = 10$  Hz (normalized frequency of 0.06 Hz) as it determined a TN of 4001 and FP of 170. While this result is good, it does not favorably compare to our MN artifact detection algorithm, which had a specificity of 100%.

#### C. AF Subject Data Result

Table III shows TPs, TNs, FPs, and FNs of AF detection before and after MN artifact elimination on six AF subjects. In the six AF subjects, TNs slightly reduced from 440082 to 409240 beats, while FPs significantly reduced from 157337 to 72018 beats; thus, specificity increased from 73.66% to 85.04%. In addition, the number of AF beats eliminated by our MN artifact algorithms was only 10 out of 56966 beats, which is 0.02%, and sensitivity slightly increased from 74.48% to 74.62%. Thus, we could increase specificity without a loss of sensitivity by using our algorithm (accuracy of 83.61%). For HPF, we found the highest accuracy of 79.97% with  $f_{\text{cut}} = 16$  Hz (normalized frequency of 0.09 Hz). Using this value, sensitivity and specificity were 74.56% and 80.78%, respectively; TP, TN, FP, and FN were 56679, 407140, 96847, and 19344, respectively.

### IV. DISCUSSION AND CONCLUSIONS

We presented a set of algorithms for robust MN artifact detection under the assumption that noise-contaminated segments exhibit random and higher variability characteristics than their noise-free counterparts. The method consists of the use of EMD to isolate the noise component of the signal followed by three statistical measures that are especially well suited to measure the

TABLE III  
TP, TN, FP, AND FN BEFORE AND AFTER MN ARTIFACT ELIMINATION BASED ON SIX AF SUBJECT DATA SETS

Data	w/ original segment				after MN artifact elimination				Elimination rate (MN artifact detection rate)
	TP	TN	FP	FN	TP	TN	FP	FN	
VIII	5430	44359	48807	9108	5420	41253	24119	9087	25.83 %
IX	2758	126444	7607	1062	2758	113559	3912	1051	12.03 %
X	13816	72123	2723	696	13816	71001	1259	688	2.90 %
XI	13603	111343	3500	935	13603	100849	1211	934	9.92 %
XII	7801	80829	17156	6737	7801	77661	9063	6636	10.10 %
XIII	13558	4984	77544	978	13558	4917	32454	949	46.55 %
Overall	56966	440082	157337	19516	56866	409240	72018	19345	
	specificity: 73.66% sensitivity: 74.48%				specificity: 85.04% sensitivity: 74.62%				

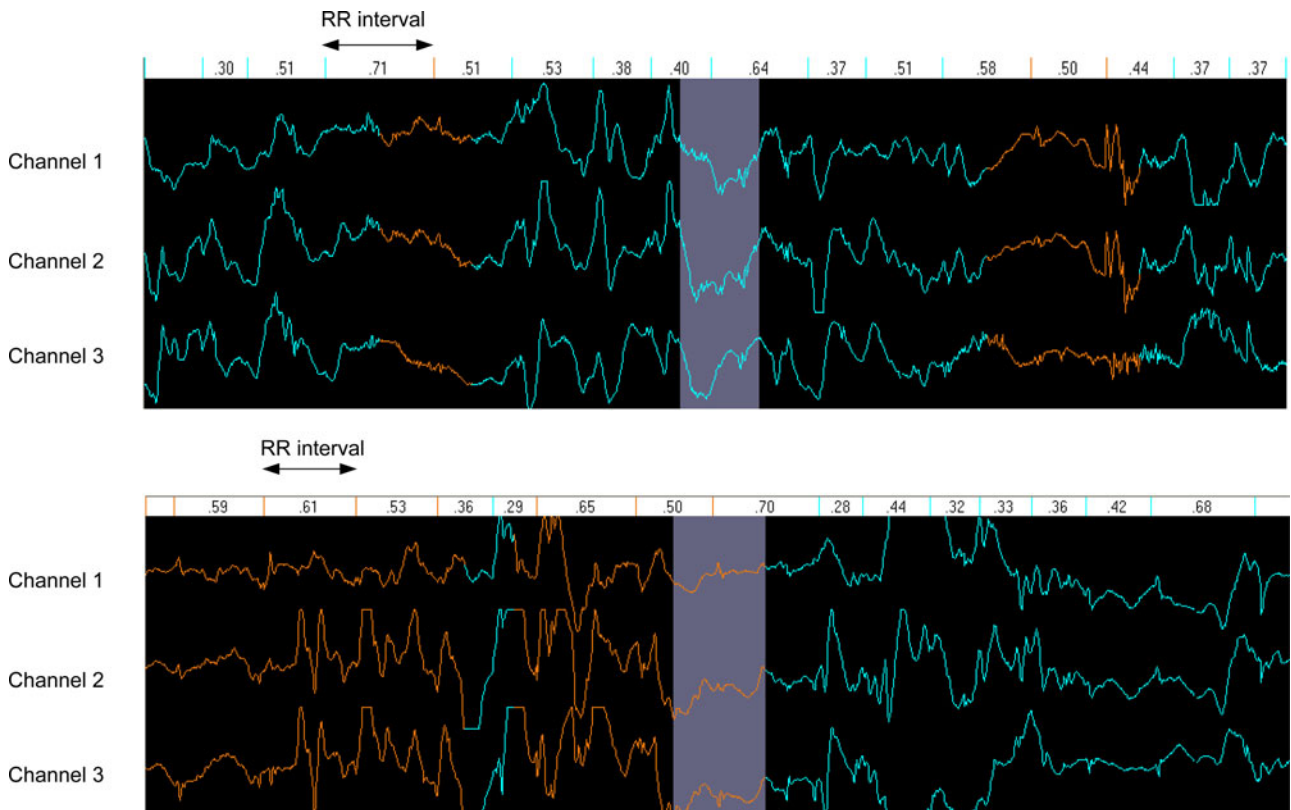


Fig. 6. Noise-contaminated ECG segments from a non-AF subject (top) and an AF subject (bottom).

signal’s complexity and variability: the Shannon entropy, mean, and variance. We found that our algorithms resulted in sensitivity of 0.9663 and specificity of 0.9473 based on 30 healthy subjects.

MN artifacts are abundant in Holter recordings, and they corrupt ECG data and interfere with accurate rhythm assessment. This is especially true with respect to identification of AF, a common and clinically- relevant cardiac arrhythmia. Thus, the goal is to identify MN artifacts using ECG data in order to avoid cardiac rhythm assessment using MN-corrupted data. Since automated AF detection is primarily based on RR interval dynam-

ics (e.g., regular for normal sinus rhythm (NSR) and irregular for AF), noise contamination of ECG segments often results in incorrect detection [1], [22]–[24]. The presence of MN artifacts is a crucial issue for both AF clinicians and engineers [25], [26]. In fact, when professional Holter data analysts interpret a subject’s data, they are taught to ignore noise-contaminated segments in order to make an accurate AF diagnosis. Thus, our method is following the guidelines already used clinically. Fig. 6 shows noise-contaminated ECG segments from a non-AF subject (top) and an AF subject (bottom), where the segments are captured from the HolterCare program supported by Scottcare

Corporation. As shown in Fig. 6, all three channels show that the ECG segments are corrupted by MN artifacts to such an extent that the correct RR interval cannot be obtained. Especially for the segment from a non-AF subject, the RR intervals are highly irregular and hence they could be mistaken as AF. Thus, it is reasonable to exclude the noise-contaminated segment in order to accurately detect fibrillation. Note that while accurate AF detection is important, it is imperative to also minimize FP detection of AF. Using this strategy, we demonstrated a significant increase in the accuracy of AF detection in 13 subjects. For these non-AF and AF subject pools, we increased the specificity from 86.96% to 100% and from 73.66% to 85.04%, respectively, without compromising the sensitivity. Further, the use of the MN artifact detection algorithm had negligible impact on those segments that were previously detected to contain AF as only 0.02% of the correct AF detections were eliminated. Should our algorithm be validated in larger cohorts with AF? We believe our real-time realizable methods will significantly improve automated AF detection using continuous ECG data, perhaps ushering in a new era of automated arrhythmia monitoring.

We can use our MN artifact method for many applications in need of discrimination between clean and noise-contaminated ECG segments. It may be possible that our MN artifact algorithms can be applied to respiratory rate estimation [27]–[30] and autonomic nervous function assessment [31] as well. In [27]–[30], the respiratory sinus arrhythmia is associated with RR intervals or heart rate variability. In [31], the sympathetic and parasympathetic nervous systems were assessed from RR intervals. Thus, incorrect RR interval detection due to MN artifacts can lead inaccurate respiratory rate and autonomic nervous function assessments. Furthermore, since our algorithms for MN artifact detection are not dependent on sensor source, the procedure has the potential to be applicable to other vital-sign sensors. For example, the photoplethysmogram (PPG) signal is a prime candidate for this application. There is ongoing research and clinical applications for deploying wearable vital sign sensors, and certainly, a PPG sensor fits this initiative as it has recently been shown to provide a wealth of vital sign information [32]–[34].

Another advantage of our algorithms is that they are real-time realizable. Specifically, using MATLAB version 2010a on a 2.66 GHz Intel Core2 processor, the computational time was 0.18–0.20 s for a 5 s data segment.

#### A. Limitations and Future Work

One potential issue with our MN artifact detection algorithm is that segment disconnectivity can occur when an identified corrupted segment is not used for subsequent AF detection. To remedy this disconnectivity, we can splice the two disconnected segments together so that AF detection can be made. However, this can potentially lead to misclassifications of the presence or absence of AF especially if there are many gaps in the required 1 min data segment. To further examine this issue, we collected 10 segments, each with 10 min duration taken from 10 non-AF subjects, and tested the AF detection algorithm by varying

disconnectivity frequency. Given each 10 min duration segment, we eliminated 5 s of data every 10, 15, 20, 25, and 30 s, and spliced them all together. It was found that all 10 segments with different disconnectivity frequencies resulted in the absence of AF. While this issue can be further examined, our preliminary analysis reveals that splicing together only those noise-free data segments does not result in false detection of AF.

Another limitation of our MN artifact detection algorithm is that the segments with saturated ECG values can often be detected as noise free. For example, ScottCare's RZ153 series recorders have an A/D dynamic voltage range between  $-2.5$  and  $+2.5$  V. If the ECG value is greater than 2.5 V due to extreme motion, the recorders show a constant 2.5 V. A consequence of this saturation effect is that the LNLTL becomes smaller, has lower variability, and less randomness than the true MN artifacts' LNLTL, thereby leading to an incorrect determination that the data are noise free. A simple remedy is to filter saturated signals prior to MN artifact detection. To further improve the MN artifact detection algorithm, probabilistic approaches such as the Bayesian classifier, hidden Markov model, or weighting training data (boosting algorithm) can be employed to examine if other IMF components can be included to further reduce artifacts.

#### REFERENCES

- [1] S. Dash, K. H. Chon, S. Lu, and E. A. Raeder, "Automatic real time detection of atrial fibrillation," *Ann. Biomed. Eng.*, vol. 37, no. 9, pp. 1701–1709, Sep. 2009.
- [2] E. J. Benjamin, P. A. Wolf, R. B. D'Agostino, H. Silbershatz, W. B. Kannel, and D. Levy, "Impact of atrial fibrillation on the risk of death: The framingham heart study," *Circulation*, vol. 98, no. 10, pp. 946–952, Sep. 1998.
- [3] S. T. Lawless, "Crying wolf: False alarms in a pediatric intensive care unit," *Crit. Care Med.*, vol. 22, no. 6, pp. 981–985, Jun. 1994.
- [4] J. Muhlsteff, O. Such, R. Schmidt, M. Perkuhn, H. Reiter, J. Lauter, J. Thijs, G. Musch, and M. Harris, "Wearable approach for continuous ECG and activity patient-monitoring," in *Proc. IEEE Conf. Eng. Med. Biol. Soc.*, 2004, vol. 3, pp. 2184–2187.
- [5] J. S. Paul, M. R. Reddy, and V. J. Kumar, "A transform domain SVD filter for suppression of muscle noise artefacts in exercise ECG's," *IEEE Trans. Biomed. Eng.*, vol. 47, no. 5, pp. 654–663, May 2000.
- [6] N. V. Thakor and Y. S. Zhu, "Applications of adaptive filtering to ECG analysis: Noise cancellation and arrhythmia detection," *IEEE Trans. Biomed. Eng.*, vol. 38, no. 8, pp. 785–794, Aug. 1991.
- [7] G. Lu, J. S. Brittain, P. Holland, J. Yianni, A. L. Green, J. F. Stein, T. Z. Aziz, and S. Wang, "Removing ECG noise from surface EMG signals using adaptive filtering," *Neurosci. Lett.*, vol. 462, no. 1, pp. 14–19, Oct. 2009.
- [8] D. L. Donoho, "De-noising by soft-thresholding," *IEEE Trans. Inf. Theory*, vol. 41, no. 1, pp. 613–627, May 1995.
- [9] M. Ayat, M. B. Shamsollahi, B. Mozaffari, and S. Kharabian, "ECG denoising using modulus maxima of wavelet transform," in *Proc. IEEE Conf. Eng. Med. Biol. Soc.*, 2009, pp. 416–419.
- [10] O. Sayadi and M. B. Shamsollahi, "ECG denoising with adaptive bionic wavelet transform," in *Proc. IEEE Conf. Eng. Med. Biol. Soc.*, 2006, pp. 6597–6600.
- [11] R. Sameni, M. B. Shamsollahi, C. Jutten, and G. D. Clifford, "A nonlinear Bayesian filtering framework for ECG denoising," *IEEE Trans. Biomed. Eng.*, vol. 54, no. 12, pp. 2172–2185, Dec. 2007.
- [12] Y. Kishimoto, Y. Kutsuna, and K. Oguri, "Detecting motion artifact ECG noise during sleeping by means of a tri-axis accelerometer," in *Proc. IEEE Conf. Eng. Med. Biol. Soc.*, 2007, pp. 2669–2672.
- [13] S. W. Yoon, S. D. Min, Y. H. Yun, S. Lee, and M. Lee, "Adaptive motion artifacts reduction using 3-axis accelerometer in e-textile ECG measurement system," *J. Med. Syst.*, vol. 32, no. 2, pp. 101–106, Apr. 2008.

- [14] N. E. Huang, Z. Shen, S. R. Long, M. L. C. Wu, H. H. Shih, Q. N. Zheng, N. C. Yen, C. C. Tung, and H. H. Liu, "The empirical mode decomposition and the Hilbert spectrum for nonlinear and non-stationary time series analysis," in *Proc. Royal Soc. London Series A, Math. Phys. Eng. Sci.*, Mar. 8, 1998, vol. 454, no. 1971, pp. 903–995.
- [15] N. ur Rehman and D. P. Mandic, "Empirical mode decomposition for trivariate signals," *IEEE Trans. Signal Process.*, vol. 58, no. 3, pp. 1059–1068, Mar. 2010.
- [16] P. L. Lee, L. Z. Shang, Y. T. Wu, C. H. Shu, J. C. Hsieh, Y. Y. Lin, C. H. Wu, Y. L. Liu, C. Y. Yang, C. W. Sun, and K. K. Shyu, "Single-trial analysis of cortical oscillatory activities during voluntary movements using empirical mode decomposition (EMD)-based spatiotemporal approach," *Ann. Biomed. Eng.*, vol. 37, no. 8, pp. 1683–1700, Aug. 2009.
- [17] B. Mijovic, M. De Vos, I. Gligorijevic, J. Taelman, and S. Van Huffel, "Source separation from single-channel recordings by combining empirical-mode decomposition and independent component analysis," *IEEE Trans. Biomed. Eng.*, vol. 57, no. 9, pp. 2188–2196, Sep. 2010.
- [18] Y. Zhang, Y. Gao, L. Wang, J. Chen, and X. Shi, "The removal of wall components in Doppler ultrasound signals by using the empirical mode decomposition algorithm," *IEEE Trans. Biomed. Eng.*, vol. 54, no. 9, pp. 1631–1642, Sep. 2007.
- [19] J. I. Salisbury and Y. Sun, "Assessment of chaotic parameters in non-stationary electrocardiograms by use of empirical mode decomposition," *Ann. Biomed. Eng.*, vol. 32, no. 10, pp. 1348–1354, Oct. 2004.
- [20] G. Rilling and P. Flandrin, "One or two frequencies? The empirical mode decomposition answers," *IEEE Trans. Signal Process.*, vol. 56, no. 1, pp. 85–95, Jan. 2008.
- [21] Z. Wu, N. E. Huang, S. R. Long, and C. K. Peng, "On the trend, detrending, and variability of nonlinear and nonstationary time series," in *Proc. Natl. Acad. Sci. USA*, Sep. 2007, vol. 104, no. 38, pp. 14889–14894.
- [22] C. Huang, S. Ye, H. Chen, D. Li, F. He, and Y. Tu, "A novel method for detection of the transition between atrial fibrillation and sinus rhythm," *IEEE Trans. Biomed. Eng.*, vol. 58, no. 4, pp. 1113–1119, Apr. 2011.
- [23] N. Kikillus, G. Hammer, N. Lentz, F. Stockwald, and A. Bolz, "Three different algorithms for identifying patients suffering from atrial fibrillation during atrial fibrillation free phases of the ECG," *Comput. Cardiol.*, vol. 34, pp. 801–804, 2007.
- [24] K. Tateno and L. Glass, "Automatic detection of atrial fibrillation using the coefficient of variation and density histograms of RR and deltaRR intervals," *Med. Biol. Eng. Comput.*, vol. 39, no. 6, pp. 664–671, Nov. 2001.
- [25] L. Jordaens, R. Tavernier, N. Gorgov, H. Kindt, C. Dimmer, and D. L. Clement, "Signal-averaged P wave: Predictor of atrial fibrillation," *J. Cardiovasc. Electrophysiol.*, vol. 9, no. 8, pp. S30–S34, Aug. 1998.
- [26] L. Clavier, J. M. Boucher, R. Lepage, J. J. Blanc, and J. C. Cornily, "Automatic P-wave analysis of patients prone to atrial fibrillation," *Med. Biol. Eng. Comput.*, vol. 40, no. 1, pp. 63–71, Jan. 2002.
- [27] J. Boyle, N. Bidargaddi, A. Sarela, and M. Karunanithi, "Automatic detection of respiration rate from ambulatory single-lead ECG," *IEEE Trans. Inf. Technol. Biomed.*, vol. 13, no. 6, pp. 890–896, Nov. 2009.
- [28] S. Babaeizadeh, S. H. Zhou, S. D. Pittman, and D. P. White, "Electrocardiogram-derived respiration in screening of sleep-disordered breathing," *J. Electrocardiol.*, Sep. 2011.
- [29] P. K. Stein, S. P. Duntley, P. P. Domitrovich, P. Nishith, and R. M. Carney, "A simple method to identify sleep apnea using Holter recordings," *J. Cardiovasc. Electrophysiol.*, vol. 14, no. 5, pp. 467–473, May 2003.
- [30] C. T. Chan, P. Hanly, J. Gabor, P. Picton, A. Pierratos, and J. S. Floras, "Impact of nocturnal hemodialysis on the variability of heart rate and duration of hypoxemia during sleep," *Kidney Int.*, vol. 65, no. 2, pp. 661–665, Feb. 2004.
- [31] Y. Bai, R. T. Mahon, J. C. White, P. R. Brink, and K. H. Chon, "Impairment of the autonomic nervous function during decompression sickness in swine," *J. Appl. Physiol.*, vol. 106, no. 3, pp. 1004–1009, Mar. 2009.
- [32] K. H. Chon, S. Dash, and K. Ju, "Estimation of respiratory rate from photoplethysmogram data using time-frequency spectral estimation," *IEEE Trans. Biomed. Eng.*, vol. 56, no. 8, pp. 2054–2063, Aug. 2009.
- [33] N. Selvaraj, J. Lee, and K. H. Chon, "Time-varying methods for characterizing nonstationary dynamics of physiological systems," *Methods Inf. Med.*, vol. 49, no. 5, pp. 435–442, 2010.
- [34] B. Yang and K. H. Chon, "A novel approach to monitor nonstationary dynamics in physiological signals: Application to blood pressure, pulse oximeter, and respiratory data," *Ann. Biomed. Eng.*, vol. 38, no. 11, pp. 3478–3488, Nov. 2010.

Authors' photographs and biographies not available at the time of publication.